*Artificial Intelligence for Engineering Design, Analysis and Manufacturing*

**cambridge.org/aie**

# Prediction of the onset of shear localization based on machine learning

Samet Akar[1], Ece Aylı[1], Oğuzhan Ulucak[2] and Doruk Uğurer[3]

[1]Department of Mechanical Engineering, Çankaya University, Ankara, Türkiye; [2]Department of Mechanical Engineering, TED University, Ankara, Türkiye and [3]Department of Mechanical Engineering, Atilim University, Ankara, Türkiye

## Research Article

**Cite this article:** Akar S, Aylı E, Ulucak O, Uğurer D (2023). Prediction of the onset of shear localization based on machine learning. *Artificial Intelligence for Engineering Design, Analysis and Manufacturing* **37**, e15, 1–12. https://doi.org/10.1017/S0890060423000136

Received: 30 September 2022
Revised: 5 January 2023
Accepted: 6 May 2023

**Keywords:**
ANFIS exponential; ANN; finite element method; shear localization; Ti6Al4V

**Corresponding author:**
Samet Akar;
Email: samet.akar@cankaya.edu.tr

**Abstract**

Predicting the onset of shear localization is among the most challenging problems in machining. This phenomenon affects the process outputs, such as machining forces, surface quality, and machined part tolerances. To predict this phenomenon, analytical, experimental, and numerical methods (especially finite element analysis) are widely used. However, the limitations of each method hinder their industrial applications, demanding a reliable and time-saving approach to predict shear localization onset. Additionally, since this phenomenon largely depends on the type and parameters of the constitutive material model, any change in these parameters requires a new set of simulations, which puts further restrictions on the application of finite element modeling. This study aims to overcome the computational efficiency of the finite element method to predict the onset of shear localization when machining Ti6Al4V using machine learning methods. The obtained results demonstrate that the FCM (fuzzy c-means) clustering ANFIS (adaptive network-based fuzzy inference system) has given better results in both training and testing when it is compared to the ANN (artificial neural network) architecture with an $R^2$ of 0.9981. Regarding this, the FCM-ANFIS is a good candidate to calculate the critical cutting speed. To the best of the authors' knowledge, this is the first study in the literature that uses a machine learning tool to predict shear localization.

## Introduction

Ti6Al4V, which is known as the workhorse of the titanium industry (Leyens and Peters, 2003), is the material of choice for many applications such as biomedical, aerospace, and aeronautics, thanks to its excellent mechanical and chemical properties such as biocompatibility, high specific strength, high corrosion resistance, better fracture toughness, and fatigue behaviors (Vanderhasten et al., 2007). Although these properties make the Ti6A14V a candidate material for widespread applications, manufacturing parts from this alloy, especially when machining is used, is quite challenging. Problems such as sticking to the cutting tool due to high chemical reactivity (Umbrello, 2008; Oliaei and Karpat, 2017*a*), increased tool/workpiece, tool/chip interface temperature due to low thermal conductivity and heat dissipation capacity, which results in accelerated tool wear and short tool life make Ti6Al4V a difficult-to-machine material (Hong et al., 1993).

Another challenge of machining titanium alloys is shear localization, resulting in serrated chip formation. Serrated chip formation is a very important phenomenon that causes fluctuations in the machining forces. These fluctuations, in turn, result in vibrations, tool wear and deteriorate the surface quality of the machined components. The part tolerance and machining accuracy are also adversely affected (Komanduri and Hou, 2002). Depending on the type of material being machined, the earlier theories are based on two different mechanisms for serrated chip formation (Komanduri and Brown, 1981). The first mechanism is introduced as ductile fracture, based on the overstraining of the material under a compressive stress field. The second mechanism relies on strain localization because of thermal softening. The latter has been termed a high-speed ductile fracture (Aifantis, 1987).

In recent studies, two advanced theories describe the shear localization phenomenon. Thermo-plastic instability (a.k.a. adiabatic shear instability) has been accepted by some researchers (Komanduri and Brown, 1981; Komanduri and Hou, 2002), while some people attribute it to the crack formation and propagation within the primary deformation zone (Aifantis, 1987). The results of a study by Recht (1964) reveal that catastrophic failure occurs when the decrease in the rate of flow stress of the material due to thermal softening exceeds its increase due to the work hardening in the primary deformation zone.

Some researchers such as Recht (1964), Semiatin and Rao (1983), Bäker et al. (2002), Komanduri and Hou (2002), and Wan et al. (2012) support the adiabatic shear band (ASB) formation, while researchers like Elbestawi et al. (1996), Poulachon and Moisan (1998), and Vyas and Shaw (1999) support the crack formation and propagation theory. Different

approaches have been used to study the shear localization phenomenon of cutting titanium alloys. These approaches mainly rely on analytical solutions, experimental tests, or numerical methods, especially finite element analysis. When these three methods are compared, the widespread application of the finite element method can be observed (Tay et al., 1974; Ceretti et al., 1999; Komanduri and Hou, 2002; Calamaz et al., 2008; Umbrello, 2008; Karpat, 2010; Sima and Özel, 2010; Wan et al., 2012; Ye et al., 2014; Ducobu et al., 2015; Wang and Liu, 2015; Li et al., 2019). This is mainly due to the superior performance of the finite element model (FEM) in revealing a better and more detailed understanding of the physics behind this process. It is worth to be mentioned that, as the machining process is a very complex process that includes several physics and nonlinear behavior, the analytical methods lack revealing pertinent information, as they need many simplifications for the problem. The experimental test is quite time-consuming and costly and very much depends on the test conditions. Additionally, measuring parameters such as stress and strain distribution during the cutting process is still very difficult and even impossible.

The studies related to the shear localization available in the literature have largely focused on the geometry of the chip serration. Little work are devoted to predicting shear localization onset, where the chip's geometry changes from continuous to a shear localized (serrated) type. This transition depends on the cutting speed compared to other machining process parameters (Ye et al., 2014). The cutting speed also significantly affects the periodicity of the chip segmentation, where the nature of the chip changes from ordered (periodic) to aperiodic disordered (aperiodic) when the cutting speed decreases. Semiatin and Rao (1983) have defined the flow localization parameter ($a$) to study the shear localization onset of three different materials of commercial purity titanium (RC-70), AISI 4340 steel (35 HRC), and AISI 1045 (90 HRB). The parameter is calculated as the ratio of the normalized flow softening rate to the strain rate sensitivity. For $a$ values equal to or greater than 5 shear localization is shown to be evident. Although the authors have mentioned shear localization in Ti6Al4V titanium alloy, they did not report the shear localization onset and flow localization parameters for Ti6Al4V.

Considering the profound effect of shear localization on machining performance, cutting temperature, accelerated tool wear, plastic localization, and fluctuations in the machining force, its prediction seems to play a significant role in selecting the proper combination of machining process parameters and tool geometry. Although the finite element method is proven effective in determining the onset of shear localization, finding the critical cutting speed requires lots of simulations. Because when using finite element (FE) simulations, one has to start with a reasonable speed and then reduce it until serrated chips disappear. This procedure highly increases the computational time of prediction. Furthermore, the FE simulations largely depend on the material model parameters, the geometry of the cutting tool, and the friction at tool/chip and tool/workpiece interfaces, which means that for any change in one of these parameters, a new set of experiments are required. This high computational time generally hinders the application of predictive techniques in the industry. Therefore, the use of a computationally efficient method of predicting shear localization onset seems to be essential. For instance, Mohammed et al. (2021) used finite element analysis (FEA) and machine learning to predict the casing buckling and deformation responses of shale gas wells. Using artificial intelligence methods is quick, robust, and accurate when compared with the FEA. Also, Saldaña-Robles et al. (2020) used both FEA and ANN models to design an agricultural backhoe. They claimed that ANN decreases the number of numerical case studies and the solution time with satisfactory results. Ahmad et al. (2022) used FEA and ANN methods to predict the ultimate response of concrete columns with glass fiber-reinforced polymers. They also obtained results with a good agreement of numerical results with the experimental results and ANN results. Several researchers have been devoted to the application of machine learning methods in the field of machining. Examples could be the low-carbon machining process planning (Chen et al., 2022), prediction of surface roughness in high-pressure jet-assisted turning (Kramar et al., 2016), modeling of charge geometry and parameters on the depth of penetration in explosive cutting (Nariman–Zadeh et al., 2003), optimization of machining process parameters (Famili, 1994; Pourmostaghimi et al., 2020), development of support systems for the proper selection of machine tools and machining process parameters (Rojek, 2017), selection of the proper cutting fluids based on the machining process such as milling, grinding, honing, and lapping (Mogush et al., 1988), prediction of the micro-end mill and micro-drills failure (Sevil and Ozdemir, 2011), and development of processing resource allocations for smart workshops in cloud manufacturing and its optimization (Hui et al., 2021). However, based on the authors' knowledge, the use of machine-learning to predict the onset of shear localization has not been reported in the literature. In light of this, this study attempts to predict the onset of shear localization by an adaptive network-based fuzzy inference system (ANFIS). The network inputs are obtained using a FEM of Yılmaz and Oliaei (2020), which is shown to have a high level of accuracy in predicting shear localization onset. The authors have performed FEA simulations for various material models available in the literature and their results showed that a modified Johnson-Cook material model proposed by Sima and Özel (2010) reveals a good agreement with experimental observations. Therefore, in this study, this material model is selected and used for all simulations.

## Materials and methods

### Finite element procedure

The FEM of orthogonal cutting of Ti6Al4V has been considered, where the workpiece is modeled as an elasto-plastic material. The cutting tool is modeled as an elastic body made from cemented tungsten carbide with the properties given in Table 1. The cutting tool is modeled with a rake angle of 0°, a clearance angle of 7°, and an edge radius of 25 µm measured by laser scanning microscopy (LSM). The cutting tool geometry is selected to be the same as the tool used in the experimental verification of the FEMs of Yılmaz and Oliaei (2020) with an uncut chip thickness of 0.1 mm. The procedure to find the critical speed for the onset of shear localization starts at relatively higher speeds where chip serration occurs. Then the speed is reduced gradually until the transition from

**Table 1.** Properties of the cutting tool material (Mabrouki and Rigal, 2006)

| Density (kg/m$^3$) | Elastic modulus (GPa) | Poisson's ratio | Thermal conductivity (W/m K) | Specific heat (J/kg K) |
|---|---|---|---|---|
| 11,900 | 534 | 0.22 | 50 | 400 |

https://doi.org/10.1017/S0890060423000136 Published online by Cambridge University Press

serrated chips to continuous chips occurs. In all FEMs, the same boundary conditions and element sizes are used to obtain consistent and repeatable results for the same workpiece and cutting tool dimensions. The workpiece is meshed with 10,000 quadrilateral elements. A mesh window is defined around the edge radius of the cutting tool to have a fine mesh in the chip-forming area. The uncut chip thickness is modeled using 20 square elements, corresponding to an element edge length of 5 µm. Temperature-dependent material properties such as elastic modulus, thermal expansion, thermal conductivity, and heat capacity are used for the workpiece as given in Table 2 (Mabrouki and Rigal, 2006).

The generic boundary conditions of the FEM are shown in Figure 1. As seen, the cutting tool is fixed in $X$ and $Y$ directions while the workpiece moves toward the cutting tool with a prescribed velocity equal to the cutting speed. A heat transfer coefficient of 10,000 (W/m$^2$°C) (Calamaz et al., 2008; Wang and Liu, 2015) is used in all simulations. It is worth mentioning that different heat transfer coefficients are used in the literature to simulate orthogonal cutting processes. For instance, Calamaz et al. (2008) used a value of 20,000 (W/m$^2$°C), Karpat (2010) used a value of 10,000 (W/m$^2$°C), Sima and Özel (2010) have used 1000 (kW/m$^2$K), while Oliaei and Karpat (2017*b*) have used 5000 (W/m$^2$°C). This is mainly because the simulation time for the machining is very short. Consequently, there is not enough time for heat to diffuse into the cutting tool to obtain a real temperature distribution (Outeiro et al., 2015). Therefore, researchers have tried to tune the heat transfer coefficient to obtain reasonable outputs. Fleischer et al. (2004) and Yen et al. (2004) use the tuning of the heat transfer coefficient to accelerate the convergence time.

## Friction modeling

Friction in metal cutting at different interfaces has an important effect on machining process outputs. Coulomb friction is generally used as the friction model in machining studies. To obtain the Coulomb friction coefficient, the method explained by Guo and Chou (2004) is used. In this method, the net cutting force ($F_c^c$) and thrust force ($F_t^c$) components are obtained by subtracting ploughing forces ($F_c^p$, $F_t^p$) from measured forces ($F_c^m$, $F_t^m$). The components of the plowing forces ($F_c^p$, $F_t^p$) are obtained using the method of extrapolation to a zero uncut chip thickness. The Coulomb friction model using net cutting and thrust force components is used as follows:

$$\mu = \frac{F_c^c \sin\gamma + F_t^c \cos\gamma}{F_c^c \cos\gamma - F_t^c \sin\gamma}, \tag{1}$$

where $\gamma$ is the rake angle of the cutting tool. The average Coulomb friction coefficient between titanium alloy and tungsten carbide under dry machining conditions is found as 0.41 by using net cutting and thrust force components. The results are in close agreement with the result obtained for titanium/tungsten carbide pairs under dry sliding conditions using a pin-on-disk method reported by Niu et al. (2013).

## Material model

The constitutive material model is the core of machining simulations using finite element analysis. Two approaches can be used to model shear localization through finite element modeling. One method relies on the artificial modification of the material flow stress at a higher level of strains, while the second approach is to include a damage model in the simulation. These approaches have resulted in the development of different material models to study serrated chip formation. Yılmaz and Oliaei (2020) have conducted an extensive study to understand the capabilities of existing material models to predict shear localization onset. Based on their verified results, the modified material model proposed by Sima and Özel (2010) is shown to reveal the best results. This material model considers a temperature-dependent overarching modifier by choosing a temperature-dependent $D$ and $p$ parameters as $D = 1 - (T/T_m)^d$, and $p = (T/T_m)^b$. In this way, Sima and Özel (2010) are supposed to enhance the softening behavior of the flow stress at elevated temperatures. Their proposed material model is given in Eq. (2):

$$\sigma = [A + B\varepsilon^n]\left[1 + C\ln\frac{\dot{\varepsilon}}{\dot{\varepsilon}_0}\right]\left[1 - \left(\frac{T - T_r}{T_m - T_r}\right)^m\right] \times \left[D + (1 - D)\left[\tanh\left(\frac{1}{(\varepsilon + p)^r}\right)\right]^s\right], \tag{2}$$

where $A = 724.7$ MPa, $B = 683.1$ MPa, $n = 0.47$, $m = 1$, $S = 5$, $r = 1$, and $d = 0.5$.

## Soft computing methodology

Soft computing transforms linguistic concepts into mathematical formats for complicated engineering problems. Two main advantages of this approach are solving nonlinear problems, for which mathematical models are not available, and introducing human knowledge such as cognition and recognition. Common artificial intelligence systems are artificial neural networks (ANNs), neuro-fuzzy systems (ANFIS), fuzzy logic systems, and particle swarm optimization. In this study, ANN and ANFIS techniques are used to develop an optimization method. In this part of the study, the theory behind the artificial intelligence system is discussed by utilizing ANN and ANFIS algorithms; more results can be extracted compared to conventional numerical techniques.

### Fuzzy c-means clustering

Fuzzy c-means (FCM) is a clustering method that puts data points into one of the predetermined clusters. The working principle of FCM is computing the degree of membership function, which describes how much the data point belongs to a certain cluster. In this study, ANFIS with FCM clustering is utilized to obtain a small number of fuzzy rules (Abdulshahed et al., 2015; Altaher and BaRukab, 2017). In Figure 2, the basic structure of FCM-based ANFIS is depicted.

The FCM method classifies the $n$ vectors into fuzzy groups and determines a cluster center for each group such that the objective

**Table 2.** Temperature-dependent material properties of Ti6Al4V (Mabrouki and Rigal, 2006)

| Thermal expansion (1/°C) | Thermal conductivity (W/m/K) | Heat capacity (N/mm$^2$/°C) | Elastic modulus (MPa) |
|---|---|---|---|
| $\alpha(T) = 3\times10^{-9}T + 7\times10^{-6}$ | $\lambda(T) = 0.015T + 7.7$ | $C_p(T) = 2.7e^{0.0002T}$ | $E(T) = -57.7T + 111{,}672$ |

https://doi.org/10.1017/S0890060423000136 Published online by Cambridge University Press

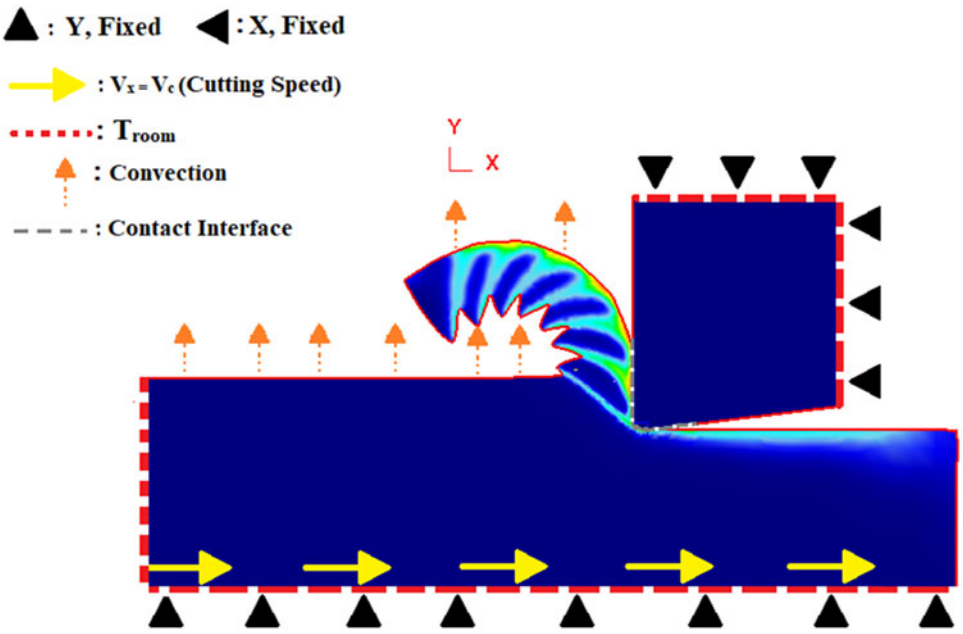


**Figure 1.** Representation of boundary conditions of the finite element model.

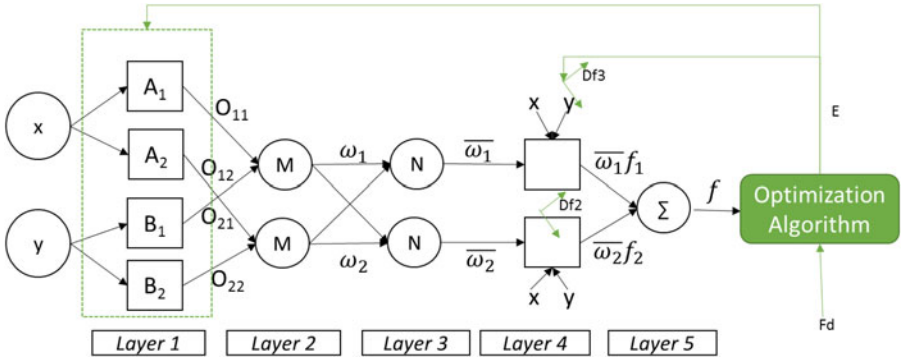


**Figure 2.** ANFIS architecture.

function of the dissimilarity measure is reduced (Abdulshahed et al., 2015). The FCM algorithm's mathematical process is given in Figure 3.

### *Adaptive network-based fuzzy inference system*

The ANFIS method was first introduced by Jang in 1993 (Jang et al., 1997). The ANFIS is a hybrid method that combines fuzzy logic with a neural network to improve system performance and predictive power based on the concept of fuzzy set theory, fuzzy if-then rules, and fuzzy reasoning (Saeed et al., 2013). In ANFIS, the training is based on the backpropagation method. In the model training phase, rule parameters and membership functions are defined. For a system that has three inputs ($x$, $y$, and $z$) and one output ($O$), a typical rule set can be defined as follows:

$$\text{Rule 1: If } (x = A_1) \text{ and } (y \text{ is } B_1), \text{ then } f_1 = p_1 x + q_1 y + r_1, \quad (3)$$

$$\text{Rule 2: If } (x = A_2) \text{ and } (y \text{ is } B_2), \text{ then } f_2 = p_2 x + q_2 y + r_2. \quad (4)$$

In these equations, $A_1$, $A_2$, $B_1$, and $B_2$ are nonlinear, and the others are linear parameters. In Figure 2, Sugeno model ANFIS structure is shown, which comprises two inputs, two rules, and one output. The fuzzy sets are characterized by membership functions. The most common membership functions are triangular, trapezoidal, Gaussian, generalized bell, and sigmoidal (Pourtousi et al., 2015). Triangular and trapezoidal MFs (membership functions) are not smooth at the corner points, whereas Gaussian and bell functions are smooth and concise. The system comprises the following five layers: fuzzification layer, product layer, normalized layer, defuzzification layer, and total output layer. The first layer is the fuzzification layer, and each node is an adaptive node with the function of (Pourtousi et al., 2015; Gupta et al., 2017):

$$O_{1,i} = \mu_{A_i}(x) \text{ for } i = 1, 2 \text{ or } O_{1,i} = \mu_{B_{i-2}}(y) \text{ for } i = 3, 4, \quad (5)$$

where $x$ and $y$ are the input at $i$th node and $\mu_{B_{i-2}}$ is the linguistic label. $O_{1,i}$ is the membership grade of fuzzy set $A$.

*Product layer:* The input of the product layer is incoming signals from the fuzzification layer and the output of this layer is given by:

$$O_{2,i} = w_i = \mu_{A_i}(x)\mu_{B_i}(y), \ i = 1, 2. \quad (6)$$

The third layer is the normalized layer that makes normalization for the weight functions that come from the product layer.

https://doi.org/10.1017/S0890060423000136 Published online by Cambridge University Press

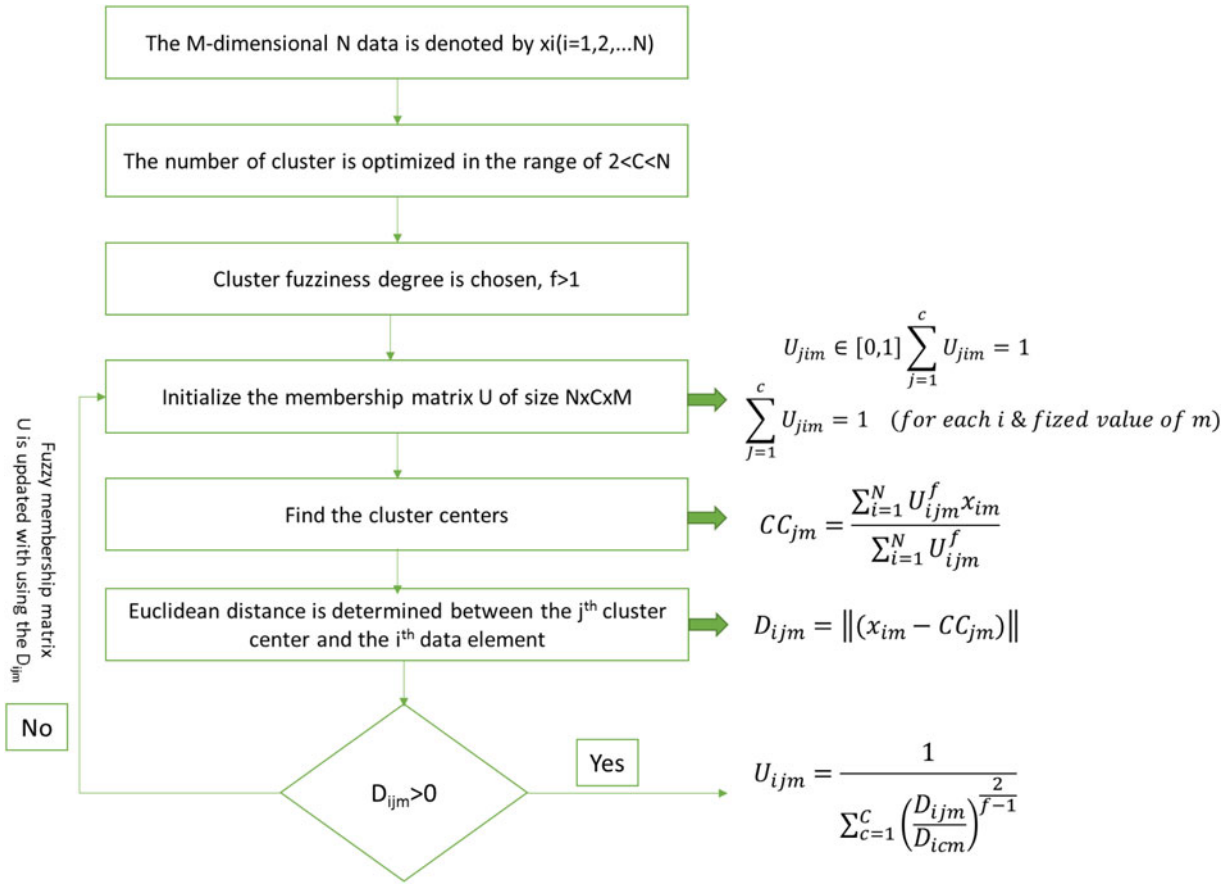


**Figure 3.** FCM algorithm steps.

The expression is given in Eq. (7):

$$O_{3,i} = \overline{w_i} = \frac{w_i}{w_1 + w_2}, \ i = 1, 2. \tag{7}$$

Layer 4 is the defuzzification layer. Every node in this layer is the adaptive node with a node function:

$$O_{4,i} = \overline{w_i} f_i = \overline{w_i}(p_i x + q_i y + r_i), \tag{8}$$

where $p_i$, $q_i$, $r_i$ are the consequent parameters. Layer 5 is the total output layer: In the output layer, there is a fixed node that makes a summation of the signals given in Eq. (9):

$$O_{5,i} = \sum_i \overline{w_i} f_i = \frac{\sum_i w_i f_i}{\sum_i w_i}. \tag{9}$$

Until Layer 4, the forward pass method is used and variables are recognized by the least-squares error estimation method. Then, using the backward pass, the error rates propagate backward. Error is calculated using the consequent parameters obtained in the third layer. The premises parameters, which are parameters of the first layer, are updated by the gradient descent. In this problem, 10 inputs related to material properties are used, and the output is the *Vc*. To predict the *Vc*, 80% of the data is used for training and the remaining 20% is used for testing the model. To detect the most favorable architecture with high performance, the exponential factor and the number of clusters are optimized in a range of $1.5 < e < 2$ and $2 <$ cluster number $< 40$, respectively, as depicted in Table 3. In this parametric study, 199 different cases are tried in the ANFIS phase. After setting the input parameters in the FCM-ANFIS model, the models are adjusted using a hybrid learning scheme. Gaussian function is selected as a membership function as it is smooth and non-zero at each point (Wang et al., 2006; Abdulshahed et al., 2013). The $R^2$ and MAPE is calculated for each trial. By varying the simulations, the best predictive model is detected.

### ANN method

ANN was introduced by McCulloch and Pitts (Wang et al., 2006) in 1943 by relating logical operations to nervous activity. ANN is inspired by the neurons in the brains of living things, which comprise a great number of neurons aligning in sequential order.

**Table 3.** Test matrix for ANFIS (adaptive network-based fuzzy inference system)

| | Exponential factor | Number of clusters |
|---|---|---|
| Case 1:39 | 1.5 | 2,3,4….40 |
| Case 40:79 | 1.6 | 2,3,4….40 |
| Case 80:119 | 1.7 | 2,3,4….40 |
| Case 120:159 | 1.8 | 2,3,4….40 |
| Case 160:199 | 1.9 | 2,3,4….40 |
| Case 200:39 | 2.0 | 2,3,4….40 |

https://doi.org/10.1017/S0890060423000136 Published online by Cambridge University Press

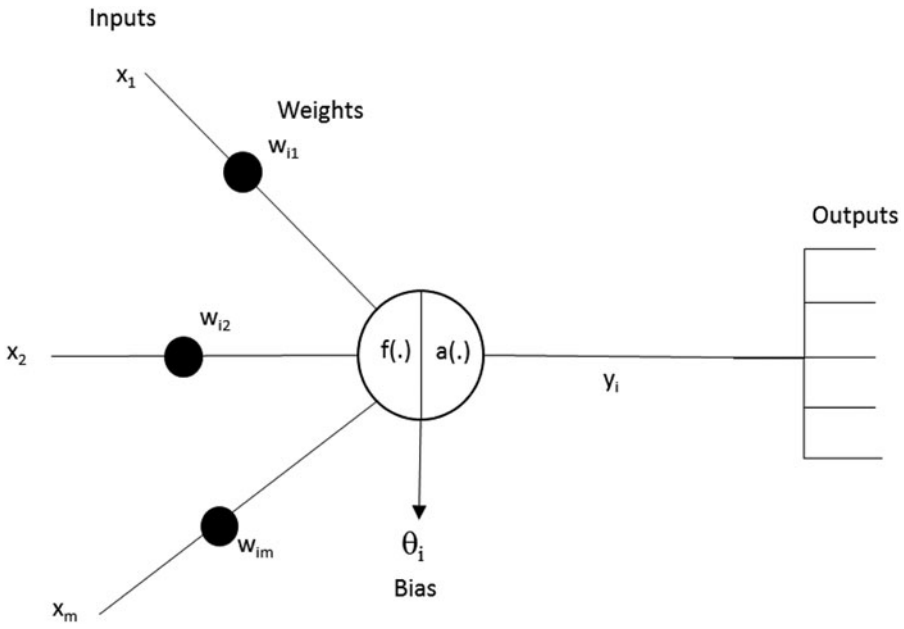


**Figure 4.** Schematic view of the ANN model (Nsaif, 2019).

Similar to our brains, neurons are connected in an order and they have a network that enables them to work together in the ANN structure. ANN, which keeps knowledge with connection weights, learns by experience and, using previous experiences, generates new values (Varol et al., 2007). ANN network is shown in Figure 4 with three inputs and several outputs. The column of neurons formed is known as layers, where the first layer is the input layer, and the last layer is the output layer. The layer between the input and output is known as the hidden layer. The input variables taken into the input layer are converted to mathematical functions in the hidden layers. In the output layer, results are given to the user (Aylı, 2020).

In the FE analysis extensively, the feed-forward backpropagation (FFBP) algorithm is used. To increase the predictive power of the ANN architecture, the number of hidden layers and the training model are two parameters that need to be optimized. The stated problem has an input layer with ten neurons, the last layer with one output in the output layer, and the layers between them are the hidden layers. The first parameter that is optimized is the number of hidden layers. The hidden layer number is varied between 1 and 15. Additionally, the effect of the training model on its performance is another parameter that is under investigation. In the Matlab user guide (Beale et al., 1992), various training algorithms are suggested for different problems. In this study, three different training models are tried: Levenberg–Marquardt, Bayesian Regularization, and Scaled Conjugate Gradient, as shown in Table 4. In total, 47 different ANN architectures are tried to find the system with the highest accuracy.

Levenberg–Marquardt (LM) algorithm is suitable for problems in which the network has fewer than 100 weights. However, in a problem with 30 hidden layer networks, the LM method is not suitable; the SCG method gives better accuracy levels and is appropriate for function approximation problems (Varol et al., 2007). LM algorithm is designed to provide second-order training speeds without using the Hessian matrix (Gang and Wang, 2013; Baghirli, 2015).

**Table 4.** ANN test case matrix (artificial neural network)

| | Number of hidden layer | Training model |
|---|---|---|
| Case 1:15 | 1,2,3….15 | Levenberg–Marquardt |
| Case 16:31 | 1,2,3….15 | Bayesian Regularization |
| Case 32:47 | 1,2,3….15 | Scaled Conjugate Gradient |

As Newton's method has higher accuracy and less computational cost, the system would like to shift toward the Newton's model as quickly as possible. For this purpose, $\mu$ is reduced in each step toward 0, and by this way, the network error function will always be reduced. In the SCG (Scaled Conjugate Gradient) model, it produces the fastest convergence while preserving error minimization. In this method, the step size is varied in each trial. The step size is determined by minimizing the performance function in each direction. Instead of using the Hessian matrix, the step size is determined by using the searching technique. The general procedure for determining the new search direction is to combine the new steepest descent direction with the previous search direction. The BR (Bayesian Regularization) method is a developed model of the LM, as this model updates the weights and bias values according to the LM method. It minimizes a combination of squared errors and weights and then determines the correct combination. To minimize the objective function, Hessian matrix calculations take place.

### *Performance evaluation*

Root mean square error (RMSE) and coefficient of determination ($R^2$) are used to evaluate the prediction ability of the machine learning techniques. There are defined as follows:

$$\mathrm{RMSE} = \sqrt{\frac{1}{N}\sum_{i=1}^{N}\left(\frac{R^{\mathrm{e}} - R^{\mathrm{p}}}{R^{\mathrm{e}}}\right)^2}, \tag{10}$$

$$R^2 = 1 - \frac{\sum_{i=1}^{N}(R_i^{\mathrm{e}} - R_i^{\mathrm{p}})^2}{\sum_{i=1}^{N}(R_i^{\mathrm{e}})^2}, \tag{11}$$

where $N$ is the number of input values. $R^{\mathrm{e}}$ denotes the exact value of the training data, while $R^{\mathrm{p}}$ is the predicted data.

https://doi.org/10.1017/S0890060423000136 Published online by Cambridge University Press

## Results and discussion

### Finite element results

A set of finite element simulations are performed to predict the critical cutting speed for various material model parameters and frictions at the tool–chip and tool–workpiece interface. Table 5 summarizes the critical cutting speed values obtained under different conditions. For each parameter, five levels are considered. The original material model parameter given by Sima and Ozel has been set as the reference value. The other levels are obtained by considering ±10% and ±20% deviation from the reference value. The reference value for the friction is used as 0.3. When all parameters are set at the reference value, a critical cutting speed of 2.8 m/min is achieved. This value has already been verified by the experimental results of Yılmaz and Oliaei (2020). This reference value has been given for each parameter for comparison.

Each parameter of the model has been studied individually, meaning that, for instance, to study parameter "*n*", it has been varied in the desired range, while all other parameters are set at reference value. In some cases, finding the critical cutting speed for the onset of shear localization required almost 15 simulations, showing the requirement for fast prediction tools.

In order to obtain the critical cutting speed, several finite element simulations are performed, where the simulations start at a higher speed where serrated chips are forming. Then, the speed was reduced until chip serration disappeared. The cutting velocity where the transition from serrated chip to continuous chip is achieved is recorded as a critical cutting speed. Figure 5 shows an example of finding the critical cutting speed for $n = 0.376$. As can be seen, the simulation is started at a cutting speed of 4 m/min, where a serrated chip has been formed, and then the speed is gradually reduced. The chip becomes continuous when

**Table 5.** Critical cutting speed for various parameters

| Parameter | | Parameter | | Parameter | |
|---|---|---|---|---|---|
| *A* | *Vc* (m/min) | *B* | *Vc* (m/min) | *C* | *Vc* (m/min) |
| 579.6 | 10.5 | 546.48 | 10.5 | 0.028 | 1.6 |
| 652.23 | 4.5 | 614.79 | 2.9 | 0.0315 | 2.65 |
| 724.7 | 2.8 | 683.1 | 2.8 | 0.035 | 2.8 |
| 797.17 | 0.95 | 751.41 | 1.9 | 0.0385 | 2.9 |
| 869.64 | 0.45 | 819.72 | 4.5 | 0.042 | 2.75 |
| Parameter | | Parameter | | Parameter | |
| *n* | *Vc* (m/min) | *m* | *Vc* (m/min) | *S* | *Vc* (m/min) |
| 0.376 | 0.65 | 0.8 | 2.1 | 4 | 4.2 |
| 0.423 | 0.75 | 0.9 | 3.3 | 4.5 | 3.7 |
| 0.47 | 2.8 | 1 | 2.8 | 5 | 2.8 |
| 0.517 | 2.4 | 1.1 | 2.4 | 5.5 | 2.5 |
| 0.564 | 1.75 | 1.2 | 1.75 | 6 | 7.5 |
| Parameter | | Parameter | | Parameter | |
| *r* | *Vc* (m/min) | *d* | *Vc* (m/min) | Friction | *Vc* (m/min) |
| 0.8 | 45 | 0.4 | 26 | 0.33 | 9 |
| 0.9 | 33 | 0.45 | 24 | 0.37 | 5 |
| 1 | 2.8 | 0.5 | 2.8 | 0.41 | 2.8 |
| 1.1 | 20 | 0.55 | 31 | 0.45 | 2.1 |
| 1.2 | 4.2 | 0.6 | 34 | 0.5 | 0.9 |

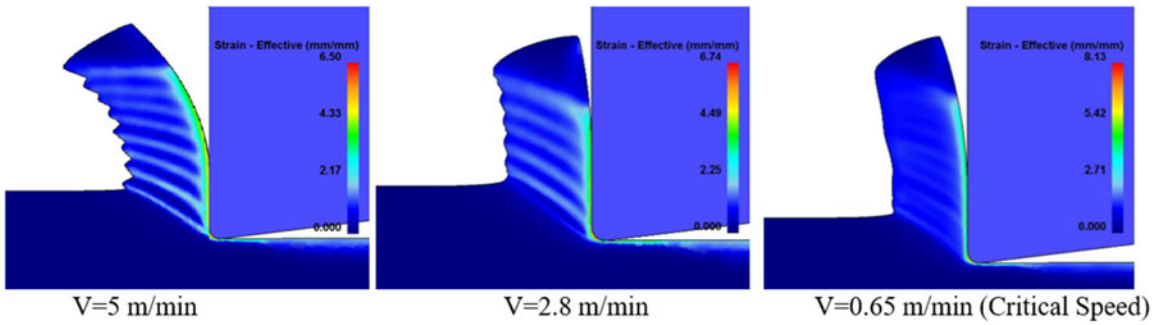


**Figure 5.** Finding the critical cutting speed for $n = 0.376$.

https://doi.org/10.1017/S0890060423000136 Published online by Cambridge University Press

the speed reaches 0.65 m/min. Figure 6 illustrates the effect of the friction coefficient on the onset of shear localization. It can be seen that at a constant speed of 2.8 m/min, as the friction coefficient increases the degree of serration also increases. This can be attributed to the heat generation at higher frictions, meaning that as more heat is deposited to the primary deformation zone, thermal softening occurs, and consequently the degree of serration increases.

### *Machine learning results*

ANN and ANFIS architectures are designed and trained to predict the cutting speed that the shear localization starts. The input layer consists of 10 inputs and the output layer contains one target. In order to determine the optimum number of hidden layers for three different learning algorithms, the number of hidden layer is varied between 1 and 15. MRE (mean relative error) is used as a statistical tool for selecting the best architecture. The results from Figure 7 shows that when the number of hidden layer is between 5 and 10 for all of the algorithms MRE decreases and $R^2$ tends to increase. Up to the number of hidden layer is equal to 13, MRE values increases for three of the method. Comparisons between the three graphics shows that the number of hidden layer trend is similar to each other whether the training model changes. After 15 hidden layers, MRE increases to the fact that the model overfits the training data and cannot generalize the

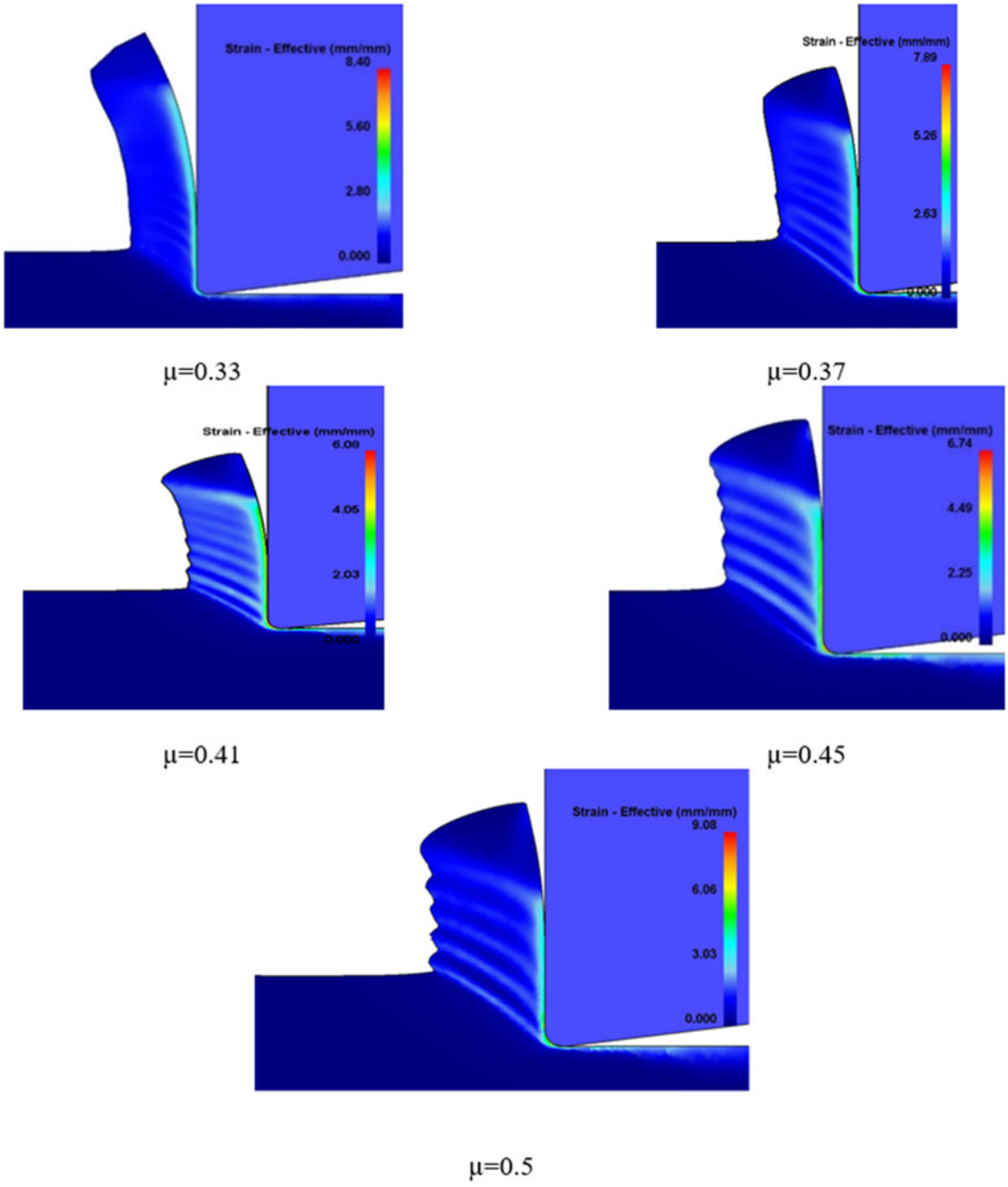


**Figure 6.** Effect of friction on serrated chip formation.

https://doi.org/10.1017/S0890060423000136 Published online by Cambridge University Press

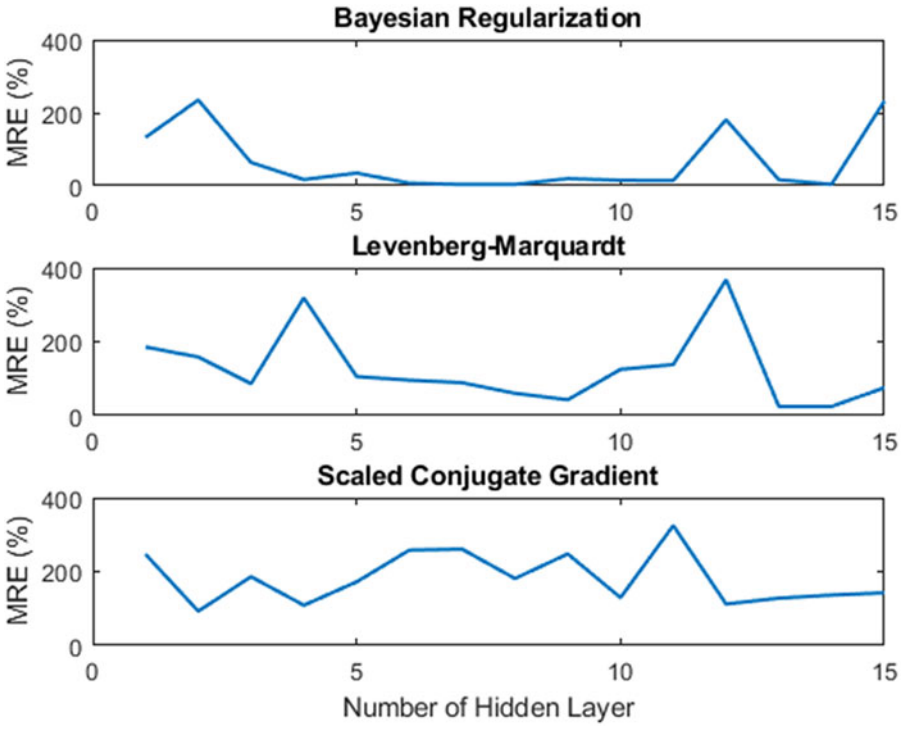


**Figure 7.** Effect of the training model and the number of hidden layer on ANN performance .

rules to new data as well. According to the statistical results, the Bayesian Regularization training model with a number of a hidden layer of 14 gives better results than other architectures.

In Figure 8, the numerical cutting velocity values are compared with the best architecture (Bayesian Regularization, number of hidden layer = 14) ANN results. The figure shows that the linear line fitted to ANN data is close to the numerical data. In other words, it is seen that, when the number of hidden layers and the training function is optimized to obtain the best architecture, the ANN model can predict the cutting velocity with new input conditions. For the best architecture, $R^2$ and RMSE values are 0.9056 and 0.913, respectively.

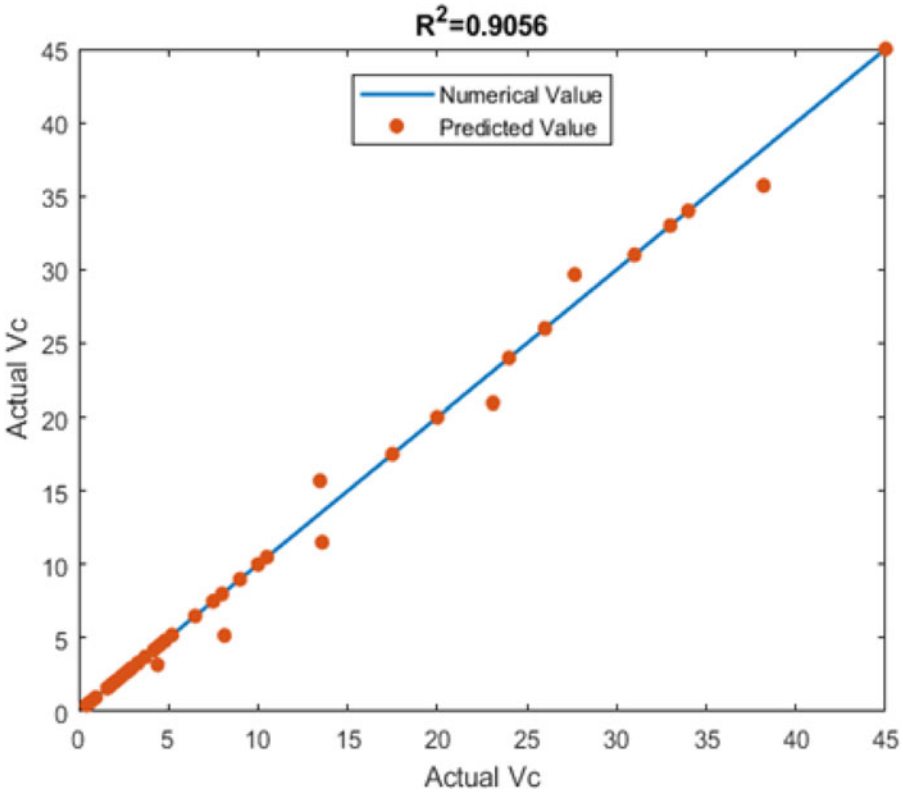


**Figure 8.** Comparison of ANN and numerical results.

https://doi.org/10.1017/S0890060423000136 Published online by Cambridge University Press

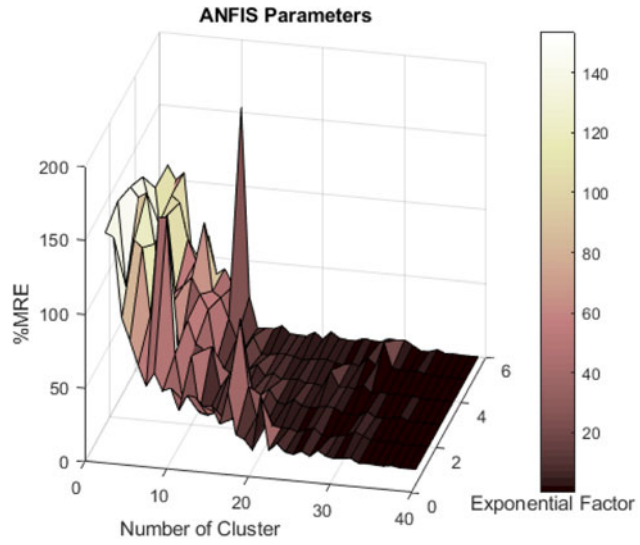


**Figure 9.** Effect of ANFIS parameters on prediction performance.

In order to obtain output with higher accuracy, different multiple ANFIS architectures are tried as it is depicted in Table 3. For each individual ANFIS architecture, exponential factor and number of cluster is varied. It is found that the Gaussian MF produced the best predictions of critical cutting speed. In Figure 9, number of cluster and exponential factor on prediction performance is shown as a function of MRE. This figure demonstrates that increasing the number of cluster decreases the MRE values and better prediction ability is achieved. For all of the tried models, convergence has been achieved after 2000 epochs. When the effect of the number of cluster to the accuracy is investigated, it is seen that cluster number effect does not have a trend. Therefore, this parameter should be optimized for each of the problems. For this problem, the number of cluster is chosen as 40 and exponential factor is 2.

**Table 6.** Performance comparison of statistical and artificial approaches

| Case number | $R^2$ | RMSE |
|---|---|---|
| ANN | 0.9038 | 0.911 |
| ANFIS | 0.9981 | 0.484 |

Figure 10 shows the accuracy of the ANFIS predictions. Testing results show that for the chosen ANFIS structure, $R^2$ is 0.998 and MRE value is reduced to 0.0064. Therefore, it can be claimed that ANFIS can reliably recognize the critical cutting speed that shear localization starts. It is important to notice that, if the architecture parameters are not optimized for each problem, the performance of the ANN and ANFIS methods will be reduced.

In Table 6, ANN and ANFIS prediction performance is compared with each other. The obtained results demonstrate that the FCM clustering ANFIS has given better results both in training and testing when it is compared to the ANN architecture with an $R^2$ of 0.9981. Regarding to this, the FCM-ANFIS is a good candidate to calculate the critical cutting speed. When the computational cost is examined, ANN time is less than the ANFIS and CFD. For 100 epochs, the time difference between ANN and ANFIS is nearly 98 s. But also, it should be noted that, although the ANFIS model predicts the critical cutting speed better and the ANN model when the appropriate MF type is not chosen, some of the ANN architectures can give better distribution than ANFIS. Therefore, optimizing the ANN and ANFIS parameters is crucial to obtain minimum error and maximum $R^2$ values.

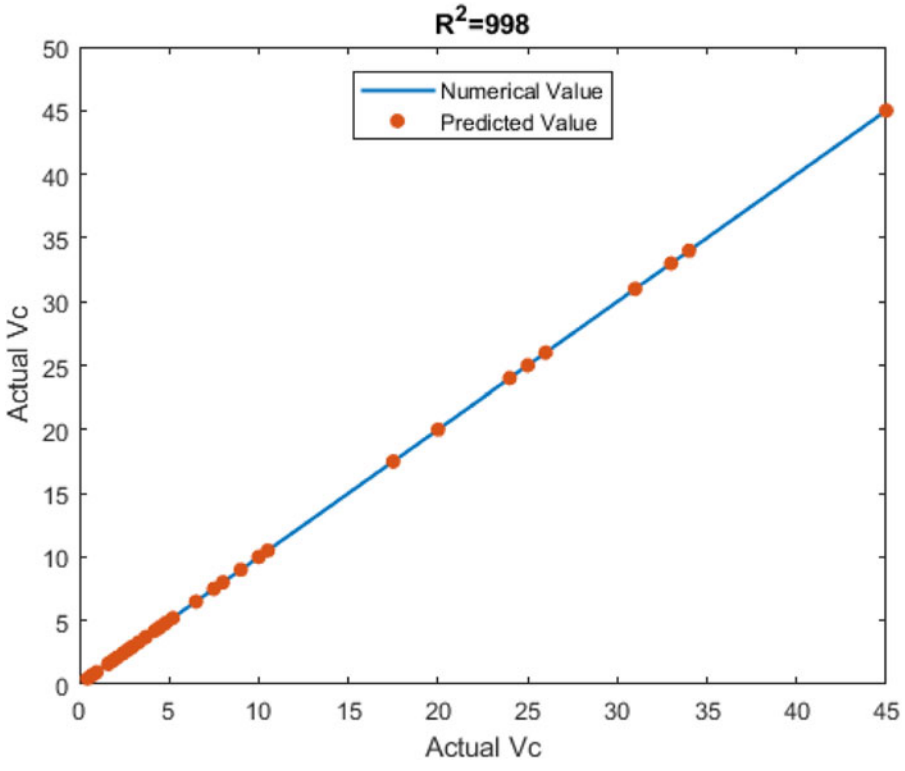


**Figure 10.** Comparison of ANFIS and numerical results.

https://doi.org/10.1017/S0890060423000136 Published online by Cambridge University Press

## Conclusions

Several FEMs are used to analyze the effect of friction and modified Johnson–Cook material model parameters on the critical speed for the onset of shear localization. Each parameter has been changed in five levels with ±10% and ±20% deviations from the reference values. It has been observed that in some situations finding the onset of shear localization requires up to 15 simulations which are quite time-consuming. Therefore, to reduce the computational cost, machine learning methods are tried to predict shear localization with high accuracy in a little time. For that purpose, ANN and ANFIS architectures are designed and trained to predict the cutting speed that the shear localization starts. The main findings can be given as follows:

- The proposed machine learning methods are shown to reveal an accurate prediction of the onset of shear localization that overcomes the computational efficiency of the finite element method.
- There is no distinct rule to develop a machine learning structure that gives the best and the most accurate results. Therefore, the effect of the critical parameters on the performance is examined. For instance, the robustness of the architecture is a function of the number of hidden layers and training models in the ANN tool.
- For ANFIS, to increase the prediction ability of the architecture, exponential factor and number of clusters should be optimized. For this problem, the number of clusters is chosen as 40 and the exponential factor is 2.
- The rapid and accurate predictive capabilities of the developed ANFIS model suggests that such models can be used for real-time optimization and control. The RMSE and $R^2$ value of the ANFIS model is 0.484 and 0.9981, respectively.
- Results demonstrate that with the increase of the friction factor, the degree of serration also increases. The reason for this situation can be be attributed to the heat generation at higher frictions, meaning that as more heat is deposited to the primary deformation zone, thermal softening occurs, and consequently the degree of serration increases.
- The time-saving aspect of soft computing for this application (and possibly other areas) is significant. Each analysis in FEA takes 5 h while 7 min for ANFIS and 5 min for ANN.

## References


**Abdulshahed A, Longstaff AP, Fletcher S and Myers A** (2013) Comparative study of ANN and ANFIS prediction models for thermal error compensation on CNC machine tools. In *Lamdamap 10th International Conference*. Euspen, pp. 79–89.

**Abdulshahed AM, Longstaff AP, Fletcher S and Myers A** (2015) Thermal error modelling of machine tools based on ANFIS with fuzzy c-means clustering using a thermal imaging camera. *Applied Mathematical Modelling* **39**, 1837–1852.

**Ahmad A, Aljuhni A, Arshid U, Elchalakani M and Abed F** (2022) Prediction of columns with GFRP bars through Artificial Neural Network and ABAQUS. In *Structures*. Elsevier, pp. 247–255.

**Aifantis EC** (1987) The physics of plastic deformation. *International Journal of Plasticity* **3**, 211–247.

**Altaher A and BaRukab O** (2017) Android malware classification based on ANFIS with fuzzy c-means clustering using significant application permissions. *Turkish Journal of Electrical Engineering and Computer Sciences* **25**, 2232–2242.

**Aylı E** (2020) Modeling of mixed convection in an enclosure using multiple regression, artificial neural network, and adaptive neuro-fuzzy interface system models. *Proceedings of the Institution of Mechanical Engineers, Part C: Journal of Mechanical Engineering Science* **234**, 3078–3093.

**Baghirli O** (2015) Comparison of Lavenberg-Marquardt, scaled conjugate gradient and Bayesian regularization backpropagation algorithms for multistep ahead wind speed forecasting using multilayer perceptron feedforward neural network.

**Bäker M, Rösler J and Siemers C** (2002) A finite element model of high speed metal cutting with adiabatic shearing. *Computers & Structures* **80**, 495–513.

**Beale MH, Hagan MT and Demuth HB** (1992) "Neural network toolbox user's guide. The MathWorks Inc, 103.

**Calamaz M, Coupard D and Girot F** (2008) A new material model for 2D numerical simulation of serrated chip formation when machining titanium alloy Ti–6Al–4V. *International Journal of Machine Tools and Manufacture* **48**, 275–288.

**Ceretti E, Lucchi M and Altan T** (1999) FEM simulation of orthogonal cutting: serrated chip formation. *Journal of Materials Processing Technology* **95**, 17–26.

**Chen Z, Zou J and Wang W** (2022) Towards comprehensive digital evaluation of low-carbon machining process planning. *AI EDAM* **36**, E21.

**Ducobu F, Rivière-Lorphèvre E and Filippi E** (2015) On the introduction of adaptive mass scaling in a finite element model of Ti6Al4V orthogonal cutting. *Simulation Modelling Practice and Theory* **53**, 1–14.

**Elbestawi MA, Srivastava AK and El-Wardany TI** (1996) A model for chip formation during machining of hardened steel. *CIRP Annals* **45**, 71–76.

**Famili A** (1994) Use of decision-tree induction for process optimization and knowledge refinement of an industrial process. *AI EDAM* **8**, 63–75.

**Fleischer J, Schmidt J, Xie LJ, Schmidt C and Biesinger F** (2004) 2D tool wear estimation using finite element method. In *Proc. of the 7th CIRP International Workshop on Modeling of Machining Operations*, pp. 82–91.

**Gang W and Wang J** (2013) Predictive ANN models of ground heat exchanger for the control of hybrid ground source heat pump systems. *Applied Energy* **112**, 1146–1153.

**Guo YB and Chou YK** (2004) The determination of ploughing force and its influence on material properties in metal cutting. *Journal of Materials Processing Technology* **148**, 368–375.

**Gupta AK, Kumar P, Sahoo RK, Sahu AK and Sarangi SK** (2017) Performance measurement of plate fin heat exchanger by exploration: ANN, ANFIS, GA, and SA. *Journal of Computational Design and Engineering* **4**, 60–68.

**Hong HATJM, Riga AT, Gahoon JM and Scott CG** (1993) Machinability of steels and titanium alloys under lubrication. *Wear* **162**, 34–39.

**Hui J, Lei J, Ding K, Zhang F and Lv J** (2021) Autonomous resource allocation of smart workshop for cloud machining orders. *AI EDAM* **35**, 226–239.

**Jang J-SR, Sun C-T and Mizutani E** (1997) Neuro-fuzzy and soft computing – a computational approach to learning and machine intelligence. *IEEE Transactions on Automatic Control* **42**, 1482–1484.

**Karpat Y** (2010) A modified material model for the finite element simulation of machining titanium alloy Ti-6Al-4 V. *Machining Science and Technology* **14**, 390–410.

**Komanduri R and Brown RH** (1981) On the mechanics of chip segmentation in machining.

**Komanduri R and Hou Z-B** (2002) On thermoplastic shear instability in the machining of a titanium alloy (Ti-6Al-4 V). *Metallurgical and Materials Transactions A* **33**, 2995–3010.

**Kramar D, Cica D, Sredanovic B and Kopac J** (2016) Design of fuzzy expert system for predicting of surface roughness in high-pressure jet assisted turning using bioinspired algorithms. *AI EDAM* **30**, 96–106.

**Leyens C and Peters M** (2003) *Titanium and Titanium Alloys: Fundamentals and Applications*. Hoboken, NJ: John Wiley & Sons.

**Li B, Zhang S, Zhang Q and Li L** (2019) Simulated and experimental analysis on serrated chip formation for hard milling process. *Journal of Manufacturing Processes* **44**, 337–348.

**Mabrouki T and Rigal J-F** (2006) A contribution to a qualitative understanding of thermo-mechanical effects during chip formation in hard turning. *Journal of Materials Processing Technology* **176**, 214–221.

**Mogush JE, Carrega D, Spirtes P and Fox MS** (1988) Treatment selection by constraint propagation: a case study in cutting fluid selection. *AI EDAM* **2**, 135–168.

**Mohammed AI, Bartlett M, Oyeneyin B, Kayvantash K and Njuguna J** (2021) An application of FEA and machine learning for the prediction and


https://doi.org/10.1017/S0890060423000136 Published online by Cambridge University Press

optimisation of casing buckling and deformation responses in shale gas wells in an in-situ operation. *Journal of Natural gas Science and Engineering* **95**, 104221.

**Nariman–Zadeh N, Darvizeh A and Dadfarmai MH** (2003) Adaptive neuro-fuzzy inference systems networks design using hybrid genetic and singular value decomposition methods for modeling and prediction of the explosive cutting process. *AI EDAM* **17**, 313–324.

**Niu QL, Zheng XH, Ming WW and Chen M** (2013) Friction and wear performance of titanium alloys against tungsten carbide under dry sliding and water lubrication. *Tribology Transactions* **56**, 101–108.

**Nsaif OS** (2019) Numerical study of the effects of geometric parameters on performance of solar chimney power plants.

**Oliaei SNB and Karpat Y** (2017*a*) Built-up edge effects on process outputs of titanium alloy micro milling. *Precision Engineering* **49**, 305–315.

**Oliaei SNB and Karpat Y** (2017*b*) Investigating the influence of friction conditions on finite element simulation of microscale machining with the presence of built-up edge. *The International Journal of Advanced Manufacturing Technology* **90**, 819–829.

**Outeiro JC, Umbrello D, M'Saoubi R and Jawahir IS** (2015) Evaluation of present numerical models for predicting metal cutting performance and residual stresses. *Machining Science and Technology* **19**, 183–216.

**Poulachon G and Moisan A** (1998) A contribution to the study of the cutting mechanisms during high speed machining of hardened steel. *CIRP Annals* **47**, 73–76.

**Pourmostaghimi V, Zadshakoyan M and Badamchizadeh MA** (2020) Intelligent model-based optimization of cutting parameters for high quality turning of hardened AISI d2. *AI EDAM* **34**, 421–429.

**Pourtousi M, Sahu JN, Ganesan P, Shamshirband S and Redzwan G** (2015) A combination of computational fluid dynamics (CFD) and adaptive neuro-fuzzy system (ANFIS) for prediction of the bubble column hydrodynamics. *Powder Technology* **274**, 466–481.

**Recht RF** (1964) Catastrophic thermoplastic shear.

**Rojek I** (2017) Technological process planning by the use of neural networks. *AI EDAM* **31**, 1–15.

**Saeed RA, Galybin AN and Popov V** (2013) 3D fluid–structure modelling and vibration analysis for fault diagnosis of Francis turbine using multiple ANN and multiple ANFIS. *Mechanical Systems and Signal Processing* **34**, 259–276.

**Saldaña-Robles AL, Bustos-Gaytán A, Diosdado-De la Peña JA, Saldaña-Robles A, Alcántar-Camarena V, Balvantín-García A and Saldaña-Robles N** (2020) Structural design of an agricultural backhoe using TA, FEA, RSM and ANN. *Computers and Electronics in Agriculture* **172**, 105278.

**Semiatin SL and Rao SB** (1983) Shear localization during metal cutting. *Materials Science and Engineering* **61**, 185–192.

**Sevil HE and Ozdemir S** (2011) Prediction of microdrill breakage using rough sets. *AI EDAM* **25**, 15–23.

**Sima M and Özel T** (2010) Modified material constitutive models for serrated chip formation simulations and experimental validation in machining of titanium alloy Ti–6Al–4V. *International Journal of Machine Tools and Manufacture* **50**, 943–960.

**Tay AO, Stevenson MG and de Vahl Davis G** (1974) Using the finite element method to determine temperature distributions in orthogonal machining. *Proceedings of the Institution of Mechanical Engineers* **188**, 627–638.

**Umbrello D** (2008) Finite element simulation of conventional and high speed machining of Ti6Al4V alloy. *Journal of Materials Processing Technology* **196**, 79–87.

**Vanderhasten M, Rabet L and Verlinden B** (2007) Deformation mechanisms of Ti-6Al-4 V during tensile behavior at low strain rate. *Journal of Materials Engineering and Performance* **16**, 208–212.

**Varol Y, Avci E, Koca A and Oztop HF** (2007) Prediction of flow fields and temperature distributions due to natural convection in a triangular enclosure using adaptive-network-based fuzzy inference system (ANFIS) and artificial neural network (ANN). *International Communications in Heat and Mass Transfer* **34**, 887–896.

**Vyas ASME and Shaw MC** (1999) Mechanics of saw-tooth chip formation in metal cutting.

**Wan ZP, Zhu YE, Liu HW and Tang Y** (2012) Microstructure evolution of adiabatic shear bands and mechanisms of saw-tooth chip formation in machining Ti6Al4V. *Materials Science and Engineering: A* **531**, 155–163.

**Wang B and Liu Z** (2015) Shear localization sensitivity analysis for Johnson–Cook constitutive parameters on serrated chips in high speed machining of Ti6Al4V. *Simulation Modelling Practice and Theory* **55**, 63–76.

**Wang K-C, Tseng P-C and Lin K-M** (2006) Thermal error modeling of a machining center using grey system theory and adaptive network-based fuzzy inference system. *JSME International Journal Series C Mechanical Systems. Machine Elements and Manufacturing* **49**, 1179–1187.

**Ye GG, Chen Y, Xue SF and Dai LH** (2014) Critical cutting speed for onset of serrated chip flow in high speed machining. *International Journal of Machine Tools and Manufacture* **86**, 18–33.

**Yen Y-C, Jain A and Altan T** (2004) A finite element analysis of orthogonal machining using different tool edge geometries. *Journal of Materials Processing Technology* **146**, 72–81.

**Yılmaz OD and Oliaei SNB** (2020) Effect of constitutive material model on the finite element simulation of shear localization onset. *Simulation Modelling Practice and Theory* **104**, 102105.

**Samet Akar** is an Associate Professor of Mechanical Engineering at Çankaya University. He holds a Ph.D. in Mechanical Engineering from Bilkent University (2016), an M.Sc. in Mechanical Engineering from the University of Tabriz (2007), and a B.Sc. in Manufacturing Engineering from the University of Applied Science and Technology (2005). His research focuses on micro machining, finite element modeling, and predictive modeling for manufacturing processes, particularly advancing precision manufacturing techniques at the microscale.

**Ece Aylı** was born in Ankara in 1989. She graduated from TED Ankara College in 2006. She got her BS, MS and PhD from TOBB University of Economics and Technology, Department of Mechanical Engineering. Dr. Ayli is currently working at Çankaya University Mechanical Engineering Department since 2017. Her area of interests are: fluid mechanics, hydro energy, supersonic flow, electronic cooling.

**Oğuzhan Ulucak** was born in Ankara in 1993. He is continuing PHD study Gazi University, Department of Mechanical Engineering. Ulucak is currently working at TED University since 2021. Area of interests are: fluid mechanics, hydro energy, water turbines, machine learning.

**Doruk Uğurer** is a 28-year-old professional currently employed as a Structural Test Engineer at Turkish Aerospace Industries. He obtained his Bachelor's degree in Mechanical Engineering from Atilim University in 2019. With a passion for continuous learning and staying updated with industry trends, Doruk is actively expanding his knowledge and skills.

https://doi.org/10.1017/S0890060423000136 Published online by Cambridge University Press